Journal of Marine Science and Technology

Volume 19 | Issue 2 Article 8

AERODYNAMIC PERFORMANCE AND SHEDDING CHARACTERISTICS ON A SWEPT-BACK WING

Shun-Chang Yen
Department of Mechanical and Mechatronic Engineering, National Taiwan Ocean University, Keelung, Taiwan, R.O.C.,
scyen@mail.ntou.edu.tw

AERODYNAMIC PERFORMANCE AND SHEDDING CHARACTERISTICS ON A SWEPT-BACK WING

Acknowledgements

This research was supported by the National Science Council of the Republic of China, under Grant No. NSC 94-2212-E-019-006.

AERODYNAMIC PERFORMANCE AND SHEDDING CHARACTERISTICS ON A SWEPT-BACK WING

Shun-Chang Yen*

Key words: swept-back wing, vortex shedding, aerodynamic coefficients.

ABSTRACT

A NACA 0012 finite swept-back wing with a sweep-back angle of 15° was utilized to investigate the effects of angle of attack (α) and the chord Reynolds number (Re_c) on the vortex shedding and aerodynamic coefficients. A hot-wire anemometer was applied to measure the vortex-shedding frequency. The projected Strouhal number (St_d) at various angles of attack was determined and discussed. The relationship between St_d and α is regressed as: $St_d = -0.0008\,\alpha + 0.209$, for $22° < \alpha < 90°$. Four characteristic surface-flow patterns: separation bubble, leading-edge bubble, bubble burst, and turbulent separation were classified by changing α and Re. The behavior of surface-flow structures significantly affects the lift, drag, and moment coefficients. The lift coefficient (C_L) increases with α in the separation bubble and leading-edge bubble regimes. The maximum increase rate of C_L with respect to α ($d(C_L)/d\alpha$) is 1.52 π/rad. Occurring in the leading-edge bubble regime. However, the maximum increase rate of drag coefficient (C_D) with respect to α ($d(C_D)/d\alpha$) is 0.49 π/rad. Occurring in the bubble-burst regime. The steep-drop of moment coefficient at stall in the unswept-wings is not observed in the swept-back wings.

I. INTRODUCTION

Many physical phenomena, such as separation, reattachment, separation bubble, vortex, etc., evolve on the wing suction surface. The aerodynamic performance is closely related to the boundary flow patterns on wing surfaces. Fig. 1 depicts the vortex shedding behavior behind a swept-back wing and the coordinate system used in this study. The bubble generally extends a large portion of wing surface and significantly changes the pressure distribution. Consequently, the aerodynamic performance is significantly changed. Mueller *et al*. [6, 7] experimentally studied the hysteresis loop in the curve of lift coefficient at low Reynolds number (*Re*) using a Lissaman 7769, Miley M06-13-128, and NACA 63_3-018 airfoils. Huang *et al*. [5] studied the aerodynamic performance by changing the surface-flow mode on a NACA 0012 airfoil. They found that the highest slope of lift coefficient (C_L) occurs in the laminar separation regime and the increase rate of C_L decreases in the separation-bubble regime. In addition, the drag coefficient (C_D) slightly decreases in the laminar separation regime, remains almost a constant in the separation-bubble regime and increases in the transition regime. Furthermore, the stall occurs in the turbulent separation regime.

The stable vortex shedding behind a swept-back wing is initialized by a complex vortex on the wing surface and the unsteady flow behind the airfoil significantly affects the wing performances. Roshko [8] found that the ordinary Strouhal number (*St*) remained constant of about 0.21, 0.18, and 0.14 for a circular cylinder, 90° wedge and flat plate, respectively, in the range of $10^3 < Re < 10^5$. The results indicated that the sharper the blockage body was, the lower the ordinary Strouhal number obtained. Zaman *et al*. [13] observed a low oscillation flow and found that the bluff-body shedding occurs at $St \approx 0.2$ during the deep stall ($\alpha \geq 18°$). However, at the onset of static stall ($\alpha \approx 15°$), the Strouhal number is lower by an order than that in the deep stall. Huang and Lin [4] investtigated the vortex shedding and shear-layer instability on a NACA 0012 wing. They revealed that the evolution of vortex shedding behind the airfoil at low angle of attack is closely related to the behavior of shear-layer instabilities. At high angles of attack, the low frequency shedding is superimposed by various high frequency shear-layer unstable waves. The characteristic modes – laminar, subcritical, transition and supercritical modes of vortex shedding were determined by changing the Reynolds number and angle of attack.

A systematic survey of surface-flow patterns on a NACA 0012 swept-back wing with $\Lambda = 15°$ for $3 \times 10^4 < Re < 1.3 \times 10^5$ was recently reported by Yen and Hsu [11]. Fig. 2 shows the distribution of surface-flow patterns obtained by Yen and Hsu. The boundary layer flow structures were visualized using the surface oil-flow scheme. Six characteristic flow regimes – *laminar separation*, *separation bubble*, *leading-*

Paper submitted 11/19/09; revised 03/08/10; accepted 03/11/10. Author for correspondence: Shun-Chang Yen (e-mail: scyen@mail.ntou.edu.tw).
**Department of Mechanical and Mechatronic Engineering, National Taiwan Ocean University, Keelung, Taiwan, R.O.C.*

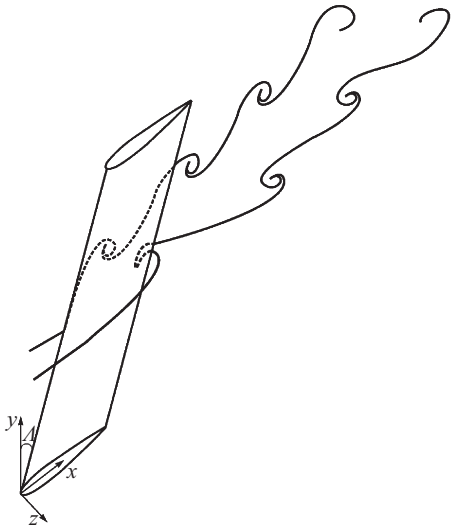

Fig. 1. Schematic diagram of flow behavior on a swept-back wing.

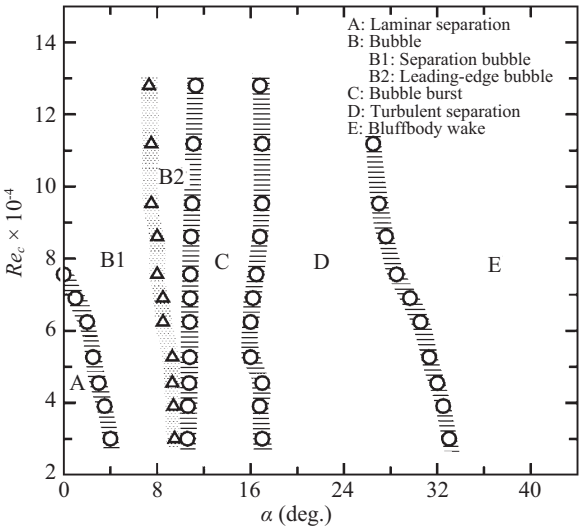

Fig. 2. Distribution of surface-flow regimes utilized in this study and Yen and Hsu [11].

edge bubble, *bubble burst*, *turbulent separation* and *bluff-body wake* were categorized and studied using various chord Reynolds numbers and angles of attack. Furthermore, the distribution of characteristic surface-flow modes are closely related to the configurations of vortex shedding behind the swept-back wing [11]. However, the properties of characteristic flow patterns and their effects on the aerodynamic performance were still not reported. In this study, the experimental results reveal the characteristic behaviors of surface-flow modes and show the effects on the aerodynamic performances and unsteady flow structures behind the swept-back wings. The objectives of this research are (1) to measure the aerodynamic coefficients by using a six component balance, (2) to study the variation of moment coefficients between the unswept and swept-back wings, and (3) to measure the vortex shedding frequency behind the swept-back wing using a hot-wire anemometer.

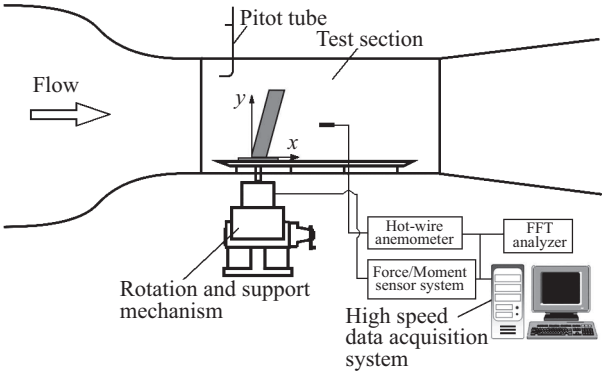

Fig. 3. Experimental setup.

II. EXPERIMENTAL SETUP

Fig. 3 shows the schematic diagram of a closed-return wind tunnel used to conduct the experiments. The test section is 60 cm × 60 cm × 120 cm in height, width and depth, respectively. A polished aluminum-alloy plate was utilized as the test-section floor and three highly transparent acrylic panels were utilized for photography and visualization. The free-stream velocity (u_∞) was measured using a Pitot-static tube. Fig. 4(a) shows the profile of turbulent intensity (*T.I.*) against u_∞. The maximum *T.I.* is < 0.2% for $0.56 < u_\infty < 40$ m/s. In addition, the non-uniformity of the average velocity across the cross-section is < 0.5%. Fig. 4(b) displays the distribution of static pressure (P_{st}-P_{atm}) as a function of u_∞. In addition, a aluminum plate with sharp leading and trailing edges was placed 50 mm over the test-section floor for controlling the boundary layer thickness. The thicknesses of boundary layer were about 4.03 mm and 1.65 mm [9] at u_∞ = 5.0 m/s and u_∞ = 30 m/s, respectively.

The material of wing model is stainless steel and the wing airfoil is NACA 0012 [1]. The sweep-back angle (Λ) is 15° used in this study. Furthermore, the chord length is 60 mm and the wing span is 300 mm which yields a full span wing aspect ratio of 10. The wing model was mounted on a support and then inset through both the test-section floor and the boundary-layer thickness controlling plate.

The vortex-shedding frequency behind the swept-back wing was detected by a TSI 1210-T1.5 hot-wire anemometer. The wire diameter and length are 5 μm and 1.5 mm to ensure the dynamic response frequency ranging from 15 to 25 kHz. The hot-wire signals were fed simultaneously to an FFT analyzer and a high speed PC-based data acquisition system. The data acquisition system embeds a sample-and-hold function for removing the phase-lag in the multi-channel acquisition. The sampling rate and the elapsed time were set at 16,000 samples/sec and 2 seconds, respectively. The aerodynamic loadings were measured using a JR^3 Universal Force-Moment

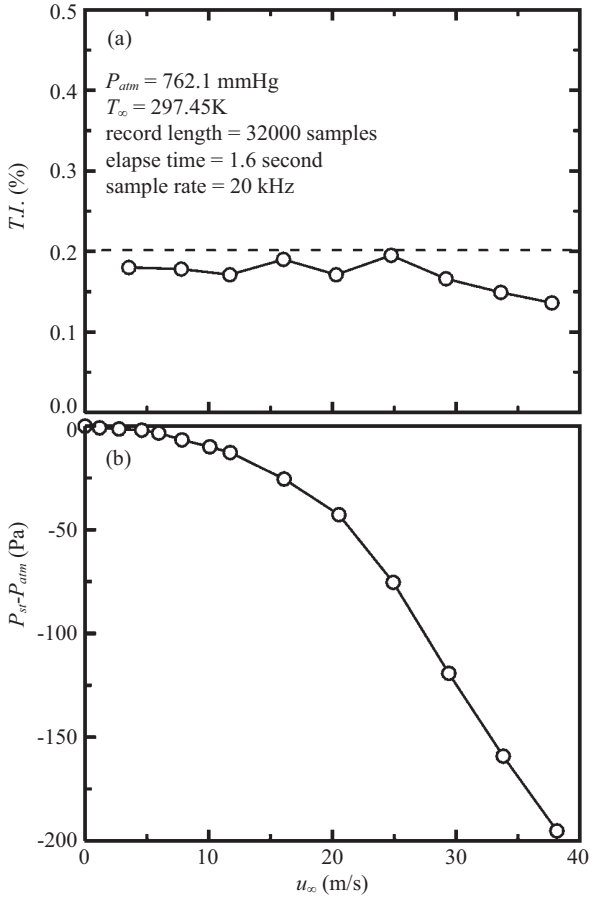

Fig. 4. Distributions of (a) turbulent intensity (*T.I.*) and (b) static pressure (P_{st}-P_{atm}) against the free stream velocity (u_∞).

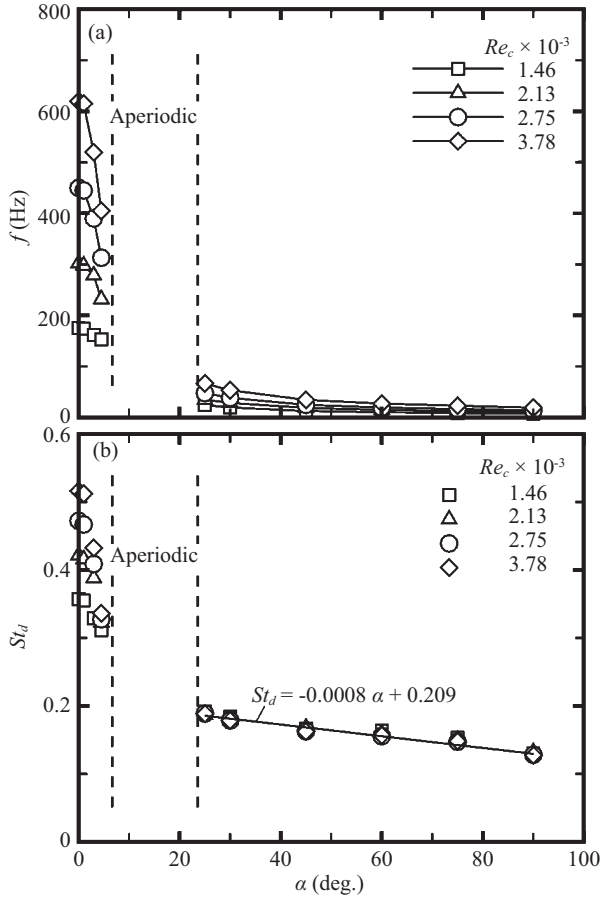

Fig. 5. Distributions of (a) vortex-shedding frequency (*f*) and (b) projected Strouhal number (St_d) versus angle of attack (α).

System. The assembly of wing model and the JR^3 Universal Force-Moment System was mounted on a rotary supporter. The resolution of this rotary supporter is 0.012 degree/div. The JR^3 balance is a six degree-of-freedom force sensor and the output electronic signals are recorded by using a PC-based high-speed data acquisition system.

The accuracy of u_∞ was affected primarily by the alignment of Pitot tube and pressure transducer. The uncertainty of u_∞ was ≈3% when a synchronized micro pressure calibration system was used and the Pitot tube was aligned carefully. The accuracy of α was controlled <0.5% and the accuracy of vortex-shedding frequency depends on the recording period of the hot-wire anemometer and the sampling rate of FFT analyzer. Therefore, the accuracies of vortex-shedding frequency, lift coefficient and drag coefficient were about ±0.75%, ±1.5% and ±2.0%, respectively.

III. RESULTS AND DISCUSSION

1. Vortex shedding

The vortex-shedding frequency (*f*) behind the swept-back wing was measured using a hot-wire probe and the output signals of hot-wire were recorded in an FFT analyzer. To remove the effects of wing junction and wingtip, the hot-wire probe was installed at $y/C = 2.5$ which is on the center section of wing span, where y is the axis in the spanwise direction. In addition, the collected signals in the x direction (along the free-stream direction) presented the similar frequency profiles. Consequently, the hot-wire probe was installed at $1 < x/C < 5$ to obtain the clear hot-wire signals. The vortex-shedding frequency varied with u_∞ was normalized using the non-dimensional parameter – projected Strouhal number ($St_d = f\,d/u_\infty$), where d is the projected chord length along the free-stream direction. Fig. 5 plots the distributions of f versus α and St_d versus α. Fig. 5(a) and (b) shows an aperiodic region occurs in the transitional regime ($7° < \alpha < 22°$) [12]. Moreover, in Fig. 5(a), the vortex-shedding frequency decreases with increasing α at various Re_c. Fig. 5(b) delineates that the maximum St_d of 0.51 occurs at $\alpha = 0°$. For $\alpha > 22°$, the St_d is not changed with Re_c and the relationship between St_d and α is regressed as follows.

$$St_d = -0.0008\,\alpha + 0.209, \text{ for } 22° < \alpha < 90°, \qquad (1)$$

where the unit of α is in degree.

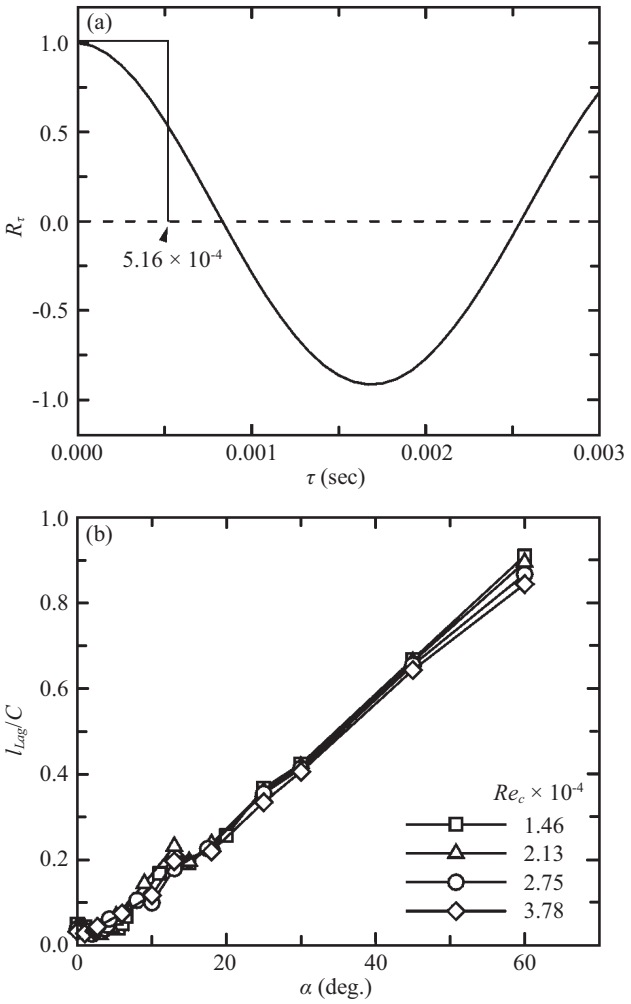

Fig. 6. Distributions of (a) autocorrelation coefficient (R_τ) versus Lagrangian integral time scale (τ) and (b) Taylor's integral length scale (l_{Lag}/C) versus angle of attack (α).

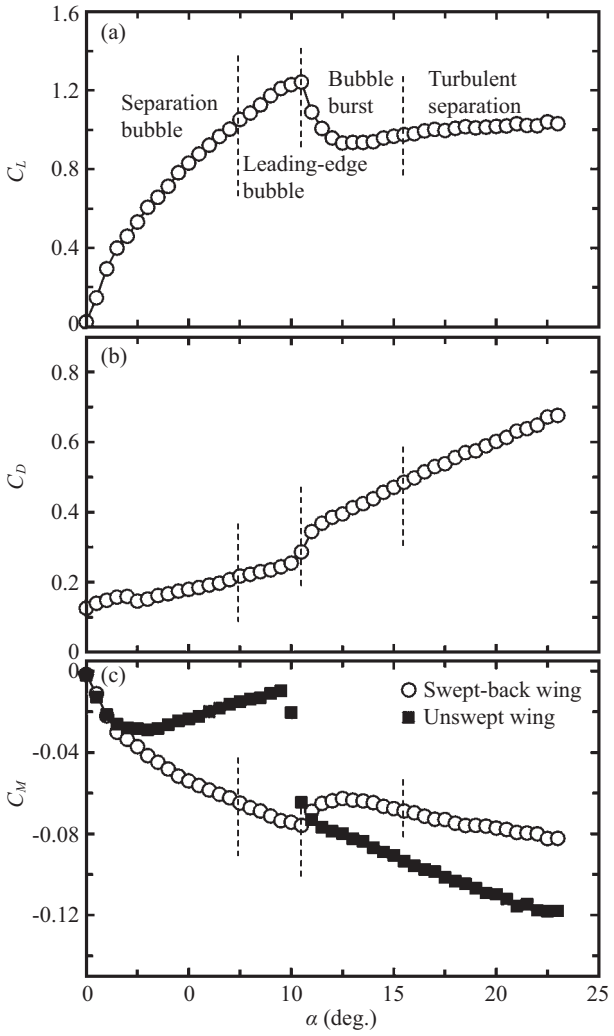

Fig. 7. Distributions of (a) lift coefficient (C_L), (b) drag coefficient (C_D) and (c) moment coefficient (C_M) against angle of attack (α) at $Re_c = 10^5$.

Fig. 6(a) depicts the autocorrelation coefficient (R_τ) against the Lagrangian integral time scale (τ). The Lagrangian integral time scale is determined from the autocorrelation data and time-averaged velocities by utilizing the Taylor's frozen flow hypothesis [10]. In addition, τ can be used to estimate the Taylor's integral length scale (l_{Lag}) of shedding vortices and turbulent fluctuations. Fig. 6(a) indicates that τ is 5.16×10^{-4}. Furthermore, Fig. 6(b) shows the distribution of the normalized Taylor's integral length scale (l_{Lag}/C) against α at various chord Reynolds numbers (Re_c). Fig. 6(b) indicates that l_{Lag}/C is positively proportional to α and the effect of Re_c on l_{Lag}/C is weak.

2. Aerodynamic performances

Fig. 7 shows the distributions of lift coefficient, drag coefficient and pitching moment coefficient (C_M) about quarter chord length against α at $Re_c = 10^5$. Fig. 7(a) shows that C_L increases monotonically with α in the separation-bubble and leading-edge bubble regimes. The maximum C_L and the increase rate of C_L with respect to α ($d(C_L)/d\alpha$) are ≈1.24 and 1.52 π/rad, respectively, occurring in the leading-edge bubble regime. The theoretical value of $d(C_L)/d\alpha$ obtained from the analytical analysis of a two-dimensional, thin, symmetric, and flat-plate airfoil in inviscid flow is 2 π/rad [2]. Abbott and van Doenhoff [1] indicated that ($d(C_L)/d\alpha$ is about 2.18 π/rad for a unswept NACA0012 wing tested in the inviscid flow. Moreover, Fig. 7(a) shows that C_L decreases when the surface flow is transited into the bubble-burst regime. In the bubble-burst regime, the reattached turbulent surface flow separates, and therefore the second separation occurs. The second separation line moves toward the leading edge with increasing α. The minimum C_L of ≈0.93 occurs in the bubble-burst regime, and then C_L increases slightly as α is further increased into the turbulent separation regime. The lift-rise phenomenon is induced from both the scavenging effect on the suction surface and the impact pressure on the pressure surface (Hoerner and Borst [3]).

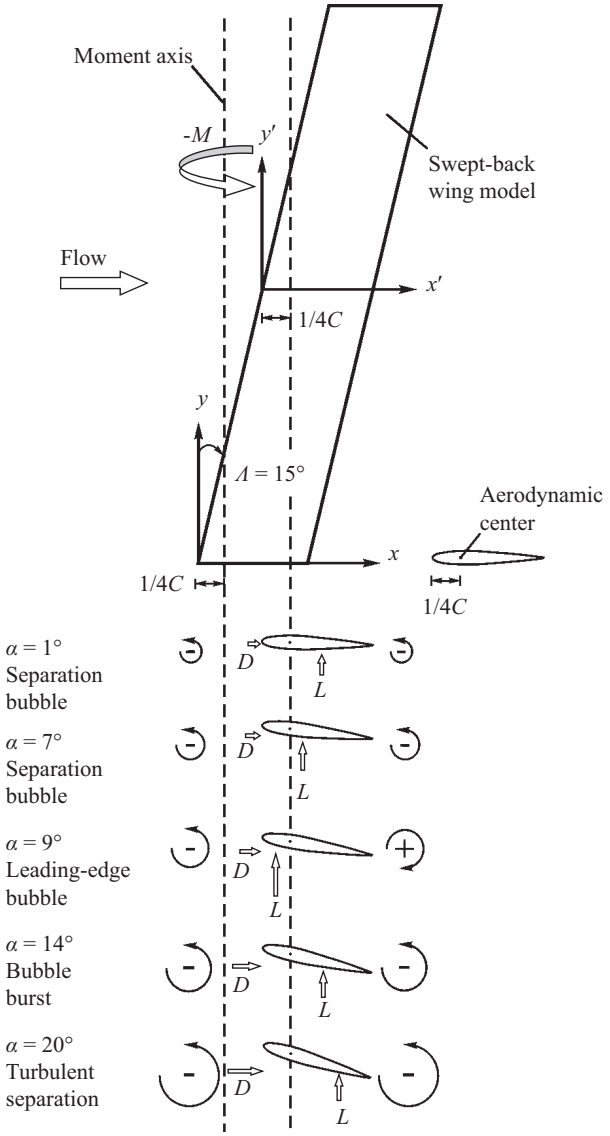

Fig. 8. Schematic diagram of lift and drag resultants and pitch-moment.

Fig. 7(b) shows the distribution of C_D against α. The bubble moves toward the leading edge and the bubble length is shrunk with increasing α. The reduction of skin friction then competes with the increase of form drag. Consequently, the C_D does not change significantly in the separation-bubble regime. In the leading-edge bubble regime, the increase of skin friction and the decrease of bubble length lead to a discontinuous rising of C_D. In the bubble-burst regime, the reattached turbulent surface flow conducts a high skin friction on the suction surface. Consequently, the maximum increase rate of C_D with respect to α ($d(C_D)/d\alpha$) of ≈0.49 π/rad occurs in the bubble-burst regime. The C_D increases almost linearly with the increase of α in the turbulent separation regime due to the significant increase of form drag.

Fig. 7(c) shows that C_M decreases as α increases for $\alpha < 10°$. In the separation bubble and leading-edge bubble regimes, the C_M increases clockwise with α due to the wing stall. The local maximum C_M occurs in the bubble-burst regime due to the increase of form drag. In the turbulent separation regime, the C_M increases clockwise with α in consequence of a large increase of form drag. However, for a unswept wing, the C_M decreases almost linearly with the increase of α for $\alpha < 2°$ while C_M increases with α for $2° < \alpha < 9°$ due to the pressure center moving toward the quarter chord point. Furthermore, the lift decreases and the pressure center moves toward the trailing edge for $\alpha > 9°$. Therefore, C_M increases with α. In addition, Fig. 7(c) shows that the steep-drop of C_M for a unswept wing is not observed in the swept-back wing.

Fig. 8 schematically plots the lift (L) and drag (D) while the moments induced from the L and D are also displayed. In the separation bubble regime ($0 < \alpha < 7.5°$), the reaction point of L moves toward the leading-edge, and both the L and D generate a counterclockwise moment. Consequently, C_M increases with α. In the leading-edge bubble regime ($7.5 < \alpha < 10°$), the reaction point of L moves toward the leading-edge and passes the aerodynamic center. Therefore, L leads a clockwise moment while D produces a counterclockwise one. Consequently, the increase rate of C_M is lowered. In the bubble-burst mode ($10° < \alpha < 16°$), the occurrence of stall conducts a sudden loss of lift and the reaction point of lift moves backward the trailing-edge. Consequently, a sudden transition of C_M curve occurs. In the turbulent separation mode ($16° < \alpha < 26°$), L generates a counterclockwise moment with respect to the aerodynamic center. In addition, D increases with α, and therefore D leads a counterclockwise moment. Consequently, the sum of counterclockwise moment induced from L and D leads a increase in C_M.

Fig. 9(a) shows the distribution of lift-drag ratio (C_L/C_D) as a function of α at $Re_c = 10^5$. In the separation-bubble regime, the C_L/C_D increases from 0 to 6.6 as α increases and the maximum C_L/C_D occurs at $\alpha = 7.5°$. In the leading-edge bubble regime, the separation bubble on the suction surface retards the increase rate of C_L/C_D, and therefore the C_L/C_D drops from 6.3 to 5.7 while α changes from 10° to 11.5°. In the bubble-burst and turbulent separation regimes, C_L/C_D decreases with the increase of α since C_L increases slightly and C_D increases rapidly in these two regimes. Fig. 9(b) shows the relationship between C_L and C_D at $Re_c = 10^5$. In the separation-bubble regime, C_D does not change significantly with C_L. However, C_D increases gradually with C_L in the leading-edge bubble regime. In bubble-burst regime, C_D increases while C_L decreases. In the turbulent separation regime, C_D changes significantly while C_L fixes approximately a constant.

IV. CONCLUSIONS

The aerodynamic performances and vortex shedding of a finite swept-back wing were experimentally studied using different angles of attack and chord Reynolds numbers. The following conclusions are drawn from the results and discussion.

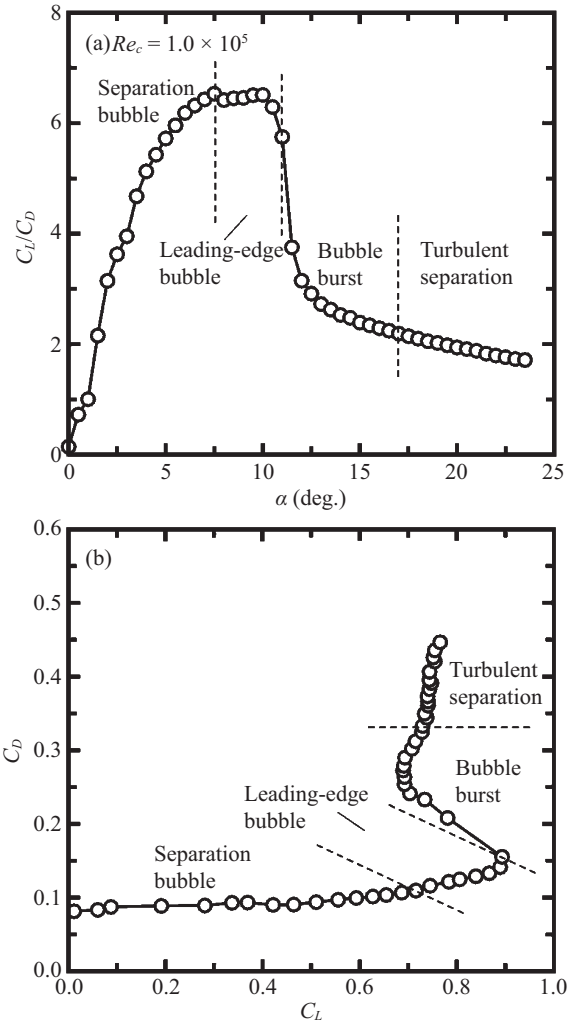

Fig. 9. Distributions of (a) lift-drag ratio (C_L/C_D) versus angle of attack (α) and (b) C_D versus C_L.

(1) The relationship between St_d and α is regressed as: $St_d = -0.0008\,\alpha + 0.209$, for $22° < \alpha < 90°$.
(2) C_L increases with α in the separation-bubble and leading-edge bubble regimes; and the maximum increase rate of C_L with respect to α is 1.52 π/rad occurring in the leading-edge bubble regime.
(3) The maximum increase rate of C_D with respect to α is 0.49 π/rad occurring in the bubble-burst regime.
(4) The steep-drop of C_M occurring at stalling point for a unswept wing is not observed by utilizing the swept-back wing.

ACKNOWLEDGMENTS

This research was supported by the National Science Council of the Republic of China, under Grant No. NSC 94-2212-E-019-006.

NOMENCLATURE

B	wing span (= 30 cm)
C	chord length (= 6 cm)
C_L	lift coefficient (= L/qbC)
C_D	drag coefficient (= D/qbC)
C_M	moment coefficient about quarter chord point (= M/qbC)
D	drag
D	projected chord length along the free-stream direction
F	vortex-shedding frequency (Hz)
L	lift
M	moment about quarter chord point
Q	dynamic pressure of free stream (= $\rho u_\infty^2/2$)
Re_c	chord Reynolds number (= $u_\infty C/\nu$)
St_d	projected Strouhal number (= $f\,d/u_\infty$)
u_∞	free stream velocity
Λ	sweep-back angle
α	angle of attack
ρ	density of air
ν	kinetic viscosity of air

REFERENCES

1. Abbott, I. H. and von Doenhoff, A. E., *Theory of Wing Section*, Dover Publications, New York, pp. 50-53 (1959).
2. Bertin, J. J. and Smith, M. L., *Aerodynamics for Engineers*, Prentice Hall, Englewood Cliffs, New Jersey, pp. 207-213 (1989).
3. Hoerner, S. F. and Borst, H. V., *Fluid Dynamic Lift*, Mrs. Liselotte A. Hoerner, Brick Town, New Jersey, (1975).
4. Huang, R. F. and Lin, C. L., "Vortex shedding and shear-layer instability of wing at low-Reynolds numbers," *AIAA Journal*, Vol. 33, No. 8, pp. 1398-1430 (1995).
5. Huang, R. F., Shy, W. W., Lin, S. W., and Hsiao, F.-B., "Influence of surface flow on aerodynamic loads of a cantilever wing," *AIAA Journal*, Vol. 34, No. 3, pp. 527-532 (1996).
6. Mueller, T. J., "The influence of laminar separation and transition on the low Reynolds number airfoil hysteresis," *Journal of Aircraft*, Vol. 22, No. 9, pp. 763-770 (1985).
7. Mueller, T. J., Pohlen, L. J., Conigliaro, P. E., and Jansen, B. J., "The influence of free-stream dimensional on low Reynolds number airfoil experiments," *Experiments in Fluids*, Vol. 1, pp. 3-14 (1983).
8. Roshko, A., "On the wake and drag of bluff bodies," *Journal of the Aerospace Science*, Vol. 22, pp. 124-135 (1955).
9. Shames, I. H., *Mechanics of Fluid*, 3rd ed., McGraw-Hill, Inc., Singapore, p. 632 (1992).
10. Tennekes, H. and Lumley, J. L., *A First Course in Turbulence*, MIT Press, Cambridge, pp. 8-103 (1972).
11. Yen, S. C. and Hsu, C. M., "Influence of boundary layer behavior on aerodynamic coefficients of a swept-back wing," *ASME Journal of Fluids Engineering*, Vol. 129, No. 6, pp. 674-681 (2007).
12. Yen, S. C. and Hsu, C. M., "Investigation on vortex shedding of a swept-back wing," *Experimental Thermal and Fluid Science*, Vol. 31, No. 8, pp. 849-855 (2007).
13. Zaman, K. B. M. Q., McKinzie, D. J., and Rumsey, C. L., "A natural low-frequency oscillation of the flow over an airfoil near stalling conditions," *Journal of Fluid Mechanics*, Vol. 202, pp. 403-442 (1989).